

000  
001  
002054  
055  
056003 **External Patch Group Prior Guided Internal Prior Learning for Real Image  
004 Denoising**057  
058  
059005  
006  
007060  
061  
062008  
009  
010063  
064  
065011  
012  
013066  
067  
068014  
015069  
070**Abstract**

For image denoising problem, the external and internal priors are playing key roles in many different methods. External priors learn from external images to restore noisy images while internal ones exploit priors of given images for denoising. The external priors are more generative and efficient on recovering structures existing in most images while the internal priors are more adaptive on recovering details existed in given noisy images. In this paper, we propose to employ the external patch group prior of images to guide the clustering of internal patch groups, and develop an external dictionary guided internal orthogonal dictionary learning algorithm for real image denoising. The internal orthogonal dictionary learning process has closed-form solutions and hence very efficient for online denoising. The experiments on standard datasets demonstrate that, that the proposed method achieves better performance than other state-of-the-art methods on real image denoising.

033  
034071  
072**1. Introduction**035  
036073  
074

Most vision systems, such as medical imaging and surveillance, need accurate feature extraction from high-quality images. The camera sensors and outdoor low light conditions will unavoidably bring noise to the captured images. The impact is that the image details will be lost or hardly visible. As a result, image denoising is an essential procedure for the reliability of these vision systems. In the research area, image denoising is also an ideal platform for testing natural image models and provides high-quality images for other computer vision tasks such as image registration, segmentation, and pattern recognition, etc.

047  
048  
049  
050  
051  
052  
053075  
076  
077  
078  
079  
080  
081  
082  
083  
084  
085  
086  
087  
088  
089  
090  
091  
092  
093  
094  
095  
096  
097  
098  
099  
100  
101  
102  
103  
104  
105  
106  
107

For several decades, there emerge numerous image denoising methods [1, 2, 3, 4, 5, 6, 7, 8, 9, 10, 11], and all of them focus mainly on dealing with additive white Gaussian noise (AWGN). In real world, the cameras will undertake high ISO settings for high-speed shots on actions, long exposure for low light on night shots, etc. Under these

situations, the noise is generated in a complex form and also been changed during the in-camera imaging pipeline [12, 13]. Therefore, the noise in real images are much more complex than Gaussian [13, 14]. It depends on camera series, brands, as well as the settings (ISO, shutter speed, and aperture, etc). The models designed for AWGN would become much less effective on real noisy images.

In the last decade, the methods of [15, 16, 17, 18, 19, 20, 13] are developed to deal with real noisy images. Almost all these methods employ a two-stage framework: estimating the parameters of the assumed noise model (usually Gaussian) and performing denoising with the help of the noise modeling and estimation in the first stage. However, the Gaussian assumption is inflexible in describing the complex noise on real noisy images [17]. Although the mixture of Gaussians (MoG) model is possible to approximate any noise distribution [21], estimating its parameters is time consuming via nonparametric Bayesian techniques [20]. To evaluate the performance of these methods on dealing with complex real noise, we apply these methods, with corresponding default parameters, on a real noisy image provided in [13]. The testing image is captured by a Nikon D800 camera when ISO is 3200. The "ground truth" image is also provided with which we can calculate objective measurements such as PSNR and SSIM [22]. The denoised images are listed in Figure 1, from which we can see that these methods either remove the noise or oversmooth the complex details in real noisy image.

The above mentioned methods can be categorized into external methods which learn priors from external images to recover noisy images, and internal ones which exploit priors of given images for denoising. The external priors in natural images are free of the high correlation between noise and signals in real noisy images, while the internal prior is adaptive to the image and can recover better the latent clean image. Combining the priors of external clean images and adaptively of internal testing images can naturally improve the performance of denoising methods, especially on real noisy images. Based on these observations, in this paper, we propose to employ the external patch group prior [10]

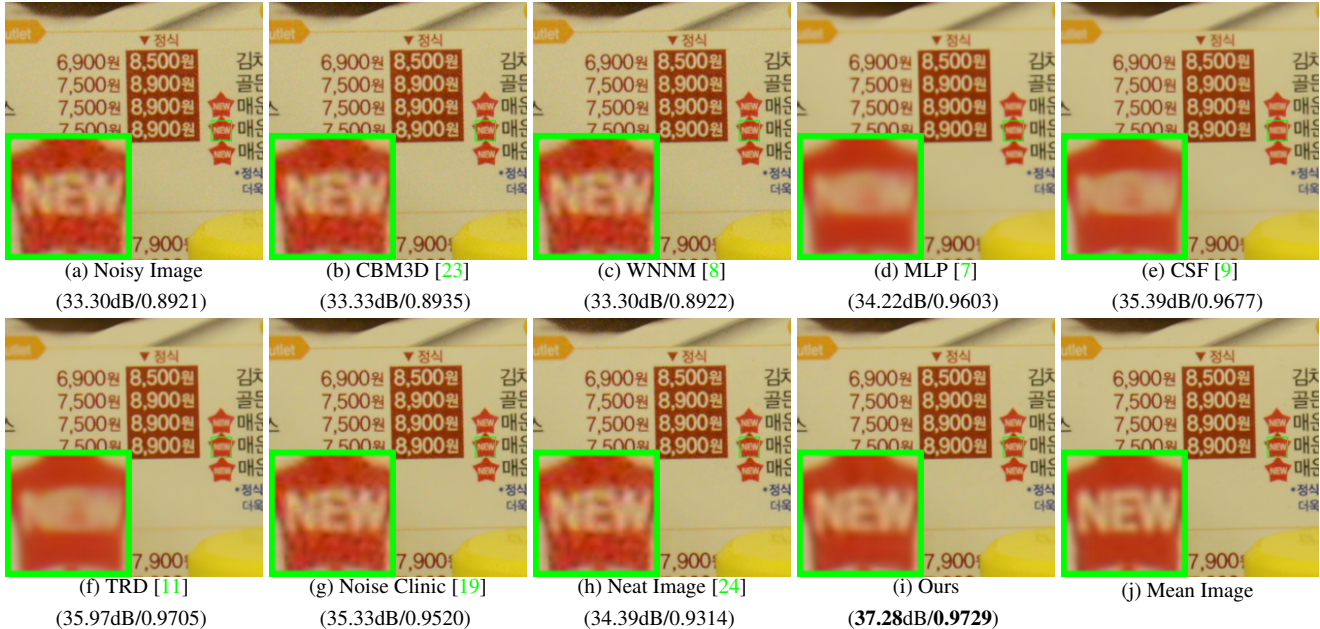


Figure 1. Denoised images of the real noisy image "Nikon D800 ISO 3200 A3" from [13] by different methods. The images are better viewed by zooming in on screen.

of natural clean images to guide the clustering of internal patch groups in given noisy image, and develop an external prior guided internal orthogonal dictionary learning (DL) algorithm for real image denoising. The internal orthogonal DL process includes two alternating stages: updating sparse coefficients and updating orthogonal dictionary. Both of the two stages have closed-form solutions. Hence, our internal DL process is very efficient for online internal denoising. Through comprehensive experiments on real noisy images captured by different cameras and settings, we demonstrate that the proposed method achieves better performance on real image denoising

## 1.1. Our Contributions

The contributions of this paper are summarized as follows:

- We propose a novel model to learn internal priors adaptive to given images. This model employs the external patch group (PG) prior learned from clean images to guide the internal PG prior learning of given images. The external prior benefits the internal learning on subspace selection and orthogonal dictionary learning.
- The proposed guided internal prior learning method is very efficient. The reason is that both the subspace selection and orthogonal dictionary learning have explicit solutions.
- For real image denoising problem, the proposed method achieves much better performance than other competing methods.

The rest of this paper will be summarized as follows: in Section 2, we briefly introduce the related work; in Section 3, we develop the proposed external prior guided internal prior learning model; in Section 4, we formulate the overall image denoising algorithm; in Section 4, we demonstrate extensive experiments on real image denoising probelm; in Section 5, we conclude our paper and give future work.

## 2. Related Work

### 2.1. Patch Group Prior of Natural Images

The Patch Group (PG) prior [10] is proposed to directly model the non-local self similar (NSS) property of natural images. The NSS property is commonly used in image restoration tasks [1, 4, 5, 8, 10]. The PG prior largely reduces the space of images to be modeled when compared to the patch prior [6]. In [10], only the PGs of clean natural images is utilized, while the PGs of noisy input images are ignored. In this paper, we make use of PGs both from external clean images and internal given real noisy image for better denoising performance.

### 2.2. Internal v.s. External Prior Learning

Learning priors to represent images has been successfully used in image modeling [3, 6, 10, 25, 33]. There are mainly two categories of prior learning methods: 1) External methods pre-learned priors (e.g., dictionaries) from a set of clean images, and the learned priors are used to recover the noisy images [6, 10]. 2) Internal methods directly learned priors from the given noisy image, and the image denoising is simultaneously done with the learning process

[3, 25, 33]. Both the two categories of methods have limitations. The external methods is not adaptive to the noisy image, while the internal methods ignores the information hidden in clean images. In this paper, our goal is to employ the external prior to guide the internal prior learning.

### 2.3. Real Image Denoising

In the last decade, there are many methods [15, 16, 17, 18, 19, 20, 13] proposed for real image denoising problem. In the seminar work of BLS-GSM [30] for real image denoising, Portilla et al. proposed to use scale mixture of Gaussian in overcomplete oriented pyramids to estimate the latent clean images. In [15], Portilla proposed to use a correlated Gaussian model for noise estimation of each wavelet subband. The work of Rabie [16] modeled the noisy pixels as outliers which are removed via Lorentzian robust estimator [31]. Liu et al. [17] proposed to use ‘noise level function’ to estimate the noise and then use Gaussian conditional random field to obtain the latent clean image. Gong et al. [18] models the noise by mixed  $\ell_1$  and  $\ell_2$  norms and remove the noise by sparsity prior in the wavelet transform domain. Later, Lebrun el al. proposed a multiscale denoising algorithm called ‘Noise Clinic’ [19]. This method generalizes the NL-Bayes model [32] to deal with blind noise and achieves state-of-the-art performance. Recently, Zhu et al. proposed a Bayesian model [20] which approximates and removes the noise via Low-Rank Mixture of Gaussians.

## 3. External Patch Group Prior Guided Internal Prior Learning

In this section, we formulate the framework of external patch group (PG) prior guided internal orthogonal dictionary learning. We first introduce the patch PG leaning on clean natural RGB images. Then we propose to employ the external PG prior to guide the internal clustering and orthogonal dictionary learning (DL). The orthogonal DL has alternative closed-form solutions in term of updating sparse coefficients and dictionary. Finally, we discuss the advantages of our proposed external PG prior guided internal orthogonal dictionary learning algorithm.

### 3.1. External Patch Group Prior Learning

Natural images often demonstrate repetitive local patterns, this nonlocal self-similarity (NSS) property is a key successful factor for many image denoising methods [1, 4, 5, 33, 8, 10]. In this section, we formulate the Patch Group prior learned on natural color images. Similar to [10], the patch group (PG) is defined as a group of similar patches to the local patch. The patch group mean is destracted, and hence different groups patches can share similar PGs. In this way, the space natural image patches to be modeled is largely reduced.

In this work, each local patch extracted from RGB images is of size  $p \times p \times 3$ . Then we search the  $M$  most similar patches  $\{\mathbf{x}_m\}_{m=1}^M$  around each local patch through Euclidean distance, in a local window of size  $W \times W$ . The  $\mathbf{x}_m \in \mathbb{R}^{3p^2 \times 1}$  is a patch vector formed by combining the 3 patch vectors (of size  $p^2 \times 1$ ) in R, G, B channels. The mean vector of this PG is  $\boldsymbol{\mu} = \frac{1}{M} \sum_{m=1}^M \mathbf{x}_m$ , and the group mean subtracted PG is defined as  $\bar{\mathbf{X}} \triangleq \{\bar{\mathbf{x}}_m = \mathbf{x}_m - \boldsymbol{\mu}\}, m = 1, \dots, M$ . Assume we have extracted  $N$  PGs from a set of external natural images, and the  $n$ -th PG is defined as  $\bar{\mathbf{X}}_n \triangleq \{\bar{\mathbf{x}}_{n,m}\}_{m=1}^M, n = 1, \dots, N$ . We employ the Gaussian Mixture Model (GMM) to learn the external patch group based NSS prior. In this model, the likelihood of the  $n$ -th PG  $\{\bar{\mathbf{X}}_n\}$  can be calculated as

$$P(\bar{\mathbf{X}}_n) = \sum_{k=1}^K \pi_k \prod_{m=1}^M \mathcal{N}(\bar{\mathbf{x}}_{n,m} | \boldsymbol{\mu}_k, \Sigma_k), \quad (1)$$

where  $K$  is the number of Gaussians and the parameters  $\pi_k$ ,  $\boldsymbol{\mu}_k$ ,  $\Sigma_k$  are mixture weight, mean vector, and covariance matrix of the  $k$ -th Gaussian, respectively. By assuming that all the PGs are independently sampled, the overall objective log-likelihood function is

$$\ln \mathcal{L} = \sum_{n=1}^N \ln \left( \sum_{k=1}^K \pi_k \prod_{m=1}^M \mathcal{N}(\bar{\mathbf{x}}_{n,m} | \boldsymbol{\mu}_k, \Sigma_k) \right). \quad (2)$$

We maximize the above objective function via EM algorithm [35] and finally obtain the GMM model with learned parameters. Similar to [10], the mean vector of each cluster is natural zeros, i.e.,  $\boldsymbol{\mu}_k = \mathbf{0}$ .

Until now, we have clustered the PGs extracted from external clean images into  $K$  subspaces (Gaussians). In order to better characterize each subspace, we perform singular value decomposition (SVD) on the covariance matrix of each subspace:

$$\boldsymbol{\Sigma} = \mathbf{U}_e \mathbf{S}_e \mathbf{V}_e^T, \quad (3)$$

and the singular vectors in  $\mathbf{U}_e$  are employed as the learned external orthogonal dictionary. Besides, the singular values are employed as weight prior which will be discussed in Section 4. The reason we use singular vectors  $\mathbf{U}_e$  as external dictionary is, its *mutual incoherence*  $\mu(\mathbf{D})$  [36], which is a measure of quality of dictionary (lower is better) and defined as

$$\mu(\mathbf{D}) = \max_{i=j} \frac{|\mathbf{d}_i^T \mathbf{d}_j|}{\|\mathbf{d}_i\|_2 \|\mathbf{d}_j\|_2}, \quad (4)$$

is naturally 0.

### 3.2. External Prior Guided Internal Prior Learning

After the external patch group (PG) prior is learned, we can employ it to guide the internal PG prior learning for the given testing (real noisy) image. The guidance mainly comes from two aspects. One aspect is that the external prior can guide the internal noisy PGs to be assigned to most suitable Gaussians or subspaces. And for each subspace, the other aspect is to guide the orthogonal dictionary learning of internal noisy PGs.

324

### 3.2.1 Guided Internal Subspace Selection

Given a real noisy image, we extract the noisy PGs and corresponding mean vectors. Each mean subtracted PG is defined as  $\bar{\mathbf{Y}} \triangleq \{\bar{\mathbf{x}}_m\}_{m=1}^M$ . Noted that, different from the external PGs, the mean vectors of the internal noisy PGs are saved for recovering. For adaptivity, we project the PG  $\bar{\mathbf{Y}}$  into its most suitable Gaussian component (subspace) of the GMM learned on external PGs. The subspace most suitable for  $\bar{\mathbf{Y}}$  is selected by firstly calculating the posterior probability of " $\bar{\mathbf{Y}}$  belonging to the  $k$ th Gaussian component":

$$P(k|\bar{\mathbf{Y}}) = \frac{\prod_{m=1}^M \mathcal{N}(\bar{\mathbf{y}}_m|\mathbf{0}, \Sigma_k)}{\sum_{l=1}^K \prod_{m=1}^M \mathcal{N}(\bar{\mathbf{y}}_m|\mathbf{0}, \Sigma_l)}, \quad (5)$$

and then choosing the component with the maximum A-posteriori (MAP) probability  $\ln P(k|\bar{\mathbf{Y}})$ .

### 3.2.2 Guided Internal Orthogonal Dictionary Learning

Now all internal noisy PGs have been assigned to their corresponding most suitable Gaussian components (subspaces) in  $\{\mathcal{N}(\mathbf{0}, \Sigma_k)\}_{k=1}^K$ . For the  $k$ -th subspace including internal noisy PGs, we employ the  $k$ -th Gaussian from external prior internal prior learning framework to learn the internal orthogonal dictionary and the image denoising is simultaneously done with the learning process

sparse coding in order to recover the latent clean PGs, for under which we need a suitable dictionary for coding.

can learn for each subspace an internal orthogonal dictionary adaptive to the noisy PGs.

$$\begin{aligned} & \min_{\mathbf{D}_i \in \mathbb{R}^{3p^2 \times r}, \mathbf{A} \in \mathbb{R}^{3p^2 \times MN}} \|\mathbf{Y} - [\mathbf{D}_e \mathbf{D}_i] \mathbf{A}\|_F^2 + \lambda \|\mathbf{A}\|_1 \\ & \text{s.t. } \mathbf{D}_i^T \mathbf{D}_i = \mathbf{I}_r, \mathbf{D}_e^T \mathbf{D}_i = \mathbf{0}, \end{aligned} \quad (6)$$

The singular vectors capture the statistical structures of NSS variations in natural images, while the singular values in  $\mathbf{S}$  represent the significance of these singular vectors. Fig. 4 shows the singular vectors for one Gaussian component.

Similar to the K-SVD [3], we employ an alternating iterative framework to solve the optimization problem 4. In fact, we initialize the orthogonal dictionary as  $\mathbf{D}^{(0)}$  and for  $t = 0, 1, \dots, T - 1$ , alternatively do:

**Updating Sparse Coefficients:** given the initialization orthogonal dictioanry  $\mathbf{D}_i^{(t)}$ , the sparce coefficients  $\mathbf{A}^{(t)}$  are obtained via solving

$$\mathbf{A}^{(t)} := \arg \min_{\mathbf{A} \in \mathbb{R}^{3p^2 \times MN}} \|\mathbf{Y} - [\mathbf{D}_e \mathbf{D}_i^{(t)}] \mathbf{A}\|_F^2 + \lambda \|\mathbf{A}\|_1. \quad (7)$$

This problem has closed-form solution by  $\mathbf{A}^* = T_\lambda(\hat{\mathbf{D}}^T \mathbf{Y})$ , where  $T_\lambda(\mathbf{A}) = \text{sgn}(\mathbf{A}) \odot \max(\mathbf{A}, \lambda)$  is a soft-thresholding function.

**Updating Orthogonal Dictionary:** given the sparse coefficients  $\mathbf{A}^{(0)}$ , the sparce coefficients  $\mathbf{A}^{(t)}$  are obtained via

solving

$$\begin{aligned} \mathbf{D}_i^{(t+1)} &:= \arg \min_{\mathbf{D}_i \in \mathbb{R}^{3p^2 \times r}} \|\mathbf{Y} - [\mathbf{D}_e \mathbf{D}_i] \mathbf{A}^{(t)}\|_F^2 \\ &\text{s.t. } \mathbf{D}_i^T \mathbf{D}_i = \mathbf{I}_r, \mathbf{D}_e^T \mathbf{D}_i = \mathbf{0}, \end{aligned} \quad (8)$$

Dividing the sparse coefficients  $\mathbf{A} = [\mathbf{A}_e^T \mathbf{A}_i^T]^T$ , where  $\mathbf{A}_e$  and  $\mathbf{A}_i$  denote the coefficients over external and internal dictionary  $\mathbf{D}_e$  and  $\mathbf{D}_i$ . According to the Proposition 2.2 in [34], the problem (8) has a closed-form solution  $\mathbf{D}_i^* = \mathbf{U} \mathbf{V}^T$ , where  $\mathbf{U}$  and  $\mathbf{V}$  are the orthogonal matrices obtained by the following SVD

$$(\mathbf{I} - \mathbf{D}_e \mathbf{D}_e^T) \mathbf{Y} \mathbf{A}_i^T = \mathbf{U} \Sigma \mathbf{V}^T \quad (9)$$

With these solutions, the final obtained dictionary  $\mathbf{D} = [\mathbf{D}_e \mathbf{D}_i]$  are orthogonal ictionary. This can be proved by the following equation

$$\mathbf{D}^T \mathbf{D} = \begin{pmatrix} \mathbf{D}_e^T \\ \mathbf{D}_i^T \end{pmatrix} (\mathbf{D}_e \mathbf{D}_i) = \begin{pmatrix} \mathbf{D}_e^T \mathbf{D}_e & \mathbf{D}_e^T \mathbf{D}_i \\ \mathbf{D}_i^T \mathbf{D}_e & \mathbf{D}_i^T \mathbf{D}_i \end{pmatrix} = \mathbf{I} \quad (10)$$

### 3.3. Discussions on Learning External Priors and Internal Priors

Until now, we have divided the noisy PGs into multiple internal subspaces. Here we take a deep analysis on how the external NSS prior guide the subspace learning of internal PGs. The help are at least threefold. Firstly, through MAP in (6), the external prior guides the noisy PGs to be clustered into the correct subspaces. If we cluster the noisy PGs in an automatical way, the subspaces we learned will be highly degraded by the signal dependent noise. Secondly, the guidance of external prior for internal clustering is more efficient than directly clustering the internal noisy PGs. It only needs to calculate the MAP probability via the equation (6) while the internal clustering via GMM is time-consuming on EM algorithm [35]. Thirdly, due to the correct guidance of external prior, the strucutal decomposition via SVD of each subspace is more adaptive. This will bring better denoising performance than the methods only using the external information.

Through SVD, the PGs in each internal subspace can be divided into singular vectors and singular values. The singular vectors are the basis of the corresponding subspace while the singular values reflect the importance of these basis. The basis can be used as dictionary to code the noisy PGs. And the sigular values are adaptive parameters for internal noisy PGs. We can compare the singular values of one internal subspace and the corresponding space of external PGs. The result is shown in Figure ???. From which we can see that the noisy subspace often have higher values than external space consisted of clean PGs. This gap is clearly made of the noise and can be used for image denoising in a natural way.

432 **4. The Denoising Algorithm** 486  
433434 **4.1. Fast Patch Group Searching by Integral Image** 487  
435

436 The searching of patch groups in images is inefficient 488  
437 if we search non-local similar patches to each local patch. 489  
438 To speed up the searching process and make our proposed 490  
439 method faster, we employ the technique of ‘Summed Area 491  
440 Table’ [37] for efficient PG searching. The SAT permits 492  
441 to evaluate the sum of pixel values in rectangular regions 493  
442 of the image with four operations, regardless of the region 494  
443 size. That is to say, we do not need do distance measure for 495  
444 each patch. It was first proposed under the name of summed 496  
445 area table[38] 497  
446

447 **4.2. Prior Weights for Sparse Coding** 498  
448

449 To remove the real noise, we employ the sparse coding 500  
450 framework. And in order to be adaptive to the input image, 501  
451 we employ the internal learned  $\mathbf{U}$  of each cluster as 502  
452 an adaptive dictioany to represent the structural variations 503  
453 of the PGs in that cluster. Since the  $\mathbf{U}$  is orthonormal, its 504  
454 *mutual incoherence* is naturally 0 and therefore better than 505  
455 other redundant dictionaries. 506  
456

$$\min_{\alpha} \|\bar{\mathbf{y}}_m - \mathbf{U}\alpha\|_2^2 + \sum_{i=1}^{3p^2} \lambda_i |\alpha_i|. \quad (11)$$

457 The  $i$ th entry of the regularization parameter  $\lambda_i$  513  
458

$$\lambda_i = \lambda / (\mathbf{S}_i + \varepsilon), \quad (12)$$

459 where  $\varepsilon$  is a small positive number to avoid dividing by zero. 514  
460 Since the dictionary  $\mathbf{U}$  is orthonormal, it is not difficult to 515  
461 find out that (4) has a closed-form solution (detailed derivation 516  
462 can be found in the supplementary material): 517  
463

$$\hat{\alpha} = \text{sgn}(\mathbf{U}^T \bar{\mathbf{y}}_m) \odot \max(|\mathbf{U}^T \bar{\mathbf{y}}_m| - \Lambda, 0), \quad (13)$$

464 where  $\Lambda = [\lambda_1, \lambda_2, \dots, \lambda_{3p^2}]$  is the vector of regularization 518  
465 parameter and  $\text{sgn}(\bullet)$  is the sign function,  $\odot$  means 519  
466 element-wise multiplication, and  $|\mathbf{U}^T \bar{\mathbf{y}}_m|$  is the absolute 520  
467 value of each entry of vector  $|\mathbf{U}^T \bar{\mathbf{y}}_m|$ . The closed-form 521  
468 solution makes our weighted sparse coding process very 522  
469 efficient. 523  
470

471 **4.3. The Overall Algorithm** 524  
472

473 With the solution  $\hat{\alpha}$  in (10), the clean patch in a PG can 525  
474 be estimated as  $\hat{\mathbf{x}}_m = \mathbf{D}\hat{\alpha} + \mu_y$ . Then the clean image  $\hat{\mathbf{x}}$  526  
475 can be reconstructed by aggregating all the estimated PGs. 527  
476 In practice, we could perform the above denoising 528  
477 procedures for several iterations for better denoising outputs. 529  
478 In iteration  $t$ , we use the iterative regularization strategy [39] 530  
479 to add back to the recovered image  $\hat{\mathbf{x}}^{(t-1)}$  some estimation 531  
480 residual in iteration  $t-1$ . The proposed denoising algorithm 532  
481 is summarized in Algorithm 1 (Alg. 1). 533  
482

483 **Alg. 1: External Prior Guided Internal Orthogonal 534  
484 Dictionary Learning for Denoising** 535  
485

486 **Input:** Noisy image  $\mathbf{y}$ , PG-GMM model 536  
487

488 1. Initialization:  $\hat{\mathbf{x}}^{(0)} = \mathbf{y}, \mathbf{y}^{(0)} = \mathbf{y}$ ; 537  
489

490 **for**  $t = 1 : IteNum$  **do** 538  
491

492   **for** each PG  $\mathbf{Y}$  **do** 539  
493

494     2. Calculate group mean  $\mu_y$  and form PG  $\bar{\mathbf{Y}}$ ; 540  
495

496     3. Gaussian component selection via (6); 541  
497

498     **end for** 542  
499

500     **for** each Internal Subspace **do** 543  
501

502       4. Internal Subspace Learning by (4); 544  
503

504       5. Recover each patch in all PGs via  $\hat{\mathbf{x}}_m = \mathbf{D}\hat{\alpha} + \mu_y$ ; 545  
505       **end for** 546  
506

507       6. Aggregate the recovered PGs of all subspaces to form 547  
508       the recovered image  $\hat{\mathbf{x}}^{(t)}$ ; 548  
509

510     **end for** 549  
511

512     **Output:** The recovered image  $\hat{\mathbf{x}}^{(IteNum)}$ . 550  
513



Figure 2. Some testing images in the dataset [13].



Figure 3. Some cropped images of the dataset [13].

522 **5. Experiments** 561  
523

524 In this section, we perform real image denoising experiments 562  
525 on three standard datasets. The first dataset is real 563  
526 noisy images with mean images as ground truths provided 564  
527 by [13], some samples are shown in Figure 3. The second 565  
528 dataset is provided by the website of Noise Clinic [19]. The 566  
529 third dataset is provided by the Commercial software Neat 567  
530 Image [24]. The second and third dataset do not have 568  
531 ground truth images. 569  
532

533 **5.1. Implementation Details** 570  
534

535 Our proposed method contains two stages, the external 571  
536 prior guided internal subspace learning stage and the adapt- 572  
537ive denoising stage. In the learning stage, there are 4 pa- 573  
538 rameters: the patch size  $p$ , the number of patches in a PG 574  
539  $M$ , the window size  $W$  for PG searching and the number of 575  
540

540 Table 1. Average PSNR(dB)/SSIM results of external, internal,  
 541 and guided methods on 60 cropped real noisy images in [13].  
 542

	Noisy	Offline	Online	Guided
PSNR	34.51	38.19	38.07	<b>38.55</b>
SSIM	0.8718	0.9663	0.9625	<b>0.9675</b>

543 clusters  $K$ . We set  $p = 6$  (hence the patch size is  $6 \times 6 \times 3$ ),  
 544  $M = 10$ ,  $W = 31$ ,  $K = 32$ . We extracted about 3.6 million  
 545 PGs from the Kodak PhotoCD Dataset, which includes  
 546 24 high quality color images, to train the external prior via  
 547 PG-GMM. In the denoising stage, the parameter  $\lambda = 0.002$   
 548 is used to regularize the sparse term. The  $\delta$  in iterative reg-  
 549 ularization is set as  $\delta = 0.09$ .

## 5.2. Comparison on External and Internal methods

550 In this subsection, we compared the proposed external  
 551 prior guided internal subspace learning model on real image  
 552 denoising. The three methods are evaluated on the dataset  
 553 provided in [13]. We calculate the PSNR, SSIM [22] and  
 554 visual quality of these three methods. We also compare the  
 555 speed. The PSNR and SSIM results on 60 cropped images  
 556 from [13] are listed in Table 1. The images are cropped into  
 557 size of  $500 \times 500$  for better illustration. We also compare  
 558 the three methods on visual quality in Figure 5.2. Compare  
 559 the denoised images listed in Figure 5.2 and Figure 5.2, we  
 560 can see that the Offline method is better at edges, smooth  
 561 regions while the Online method is good at complex tex-  
 562 tures. The reason is two folds. Firstly, the Offline method is  
 563 learned on clean images and hence is better at representing  
 564 edges, structuals, and smooth area. The online method is  
 565 influenced by the noise and hence some noise cannot be re-  
 566 moved. Secondly, the Online method is better at recovering  
 567 complex area sicne they could learn adaptive dictionaries  
 568 for the specific area. The Offline method cannot recover the  
 569 complex area since they did not learn the similar structures  
 570 from the external natural clean images.

## 5.3. Comparison With other Competing Methods

581 We compare with previous state-of-the-art Gaussian  
 582 noise removal methods such as BM3D [4], WNNM [8],  
 583 MLP [7], CSF [9], and the recently proposed TRD [11].  
 584 We also compare with three competing real image denois-  
 585 ing methods such as Noise Clinic, Neat Image, and the CC-  
 586 Noise method proposed recently. The commercial software  
 587 Neat Image [24] first estimates the parameters of noise via  
 588 a large flat area and then filters the noise accordingly. All  
 589 these methods need noise estimation which is vary hard to  
 590 perform if there is no uniform regions are available in the  
 591 testing image. The NeatImage will fail to perform automati-

592 cal parameters settings if there is no uniform regions.<sup>1</sup>

593 We the competing denoising methods from various re-  
 594 search directions on two datasets. Both the two datasets  
 595 comes from the [13]. The first dataset contains 17 images  
 596 of size over  $7000 \times 5000$ . Since this dataset contains repet-  
 597 itive contents across different images, we crop 60 small im-  
 598 ages of size  $500 \times 500$  from these 17 images in [13]. The  
 599 PSNR and SSIM resluts are listed in Table 3. The number  
 600 in red color and blue color means the best and second best  
 601 results, respectively. From the Table 3, we can see that the  
 602 external based method can already surpass largely the pre-  
 603 vious denoising methods. The improvement on PSNR over  
 604 the second best method, i.e., TRD, is 0.44dB. The

## 5.4. Discussion on Parameter $\lambda$

605 The proposed method only has a key parameter, namely  
 606 the regularization paramters  $\lambda$ . To demonstrate that the pro-  
 607 posed method is robust to the variance of  $\lambda$ , we vary the  
 608 parameter  $\lambda$  across a wide range and obtain the PSNR and  
 609 SSIM results as a function of the parameter  $\lambda$ . The re-  
 610 sults is shown in Figure 8, from which we can see that the  
 611 proposed method can achieve a PSNR (SSIM) over 38.5dB  
 612 (0.9660) when  $\lambda$  varies from 0.0015 to 0.0025. This shows  
 613 that the proposed method is indeed robust to the chosen of  
 614 the paramter  $\lambda$ .

## 6. Conclusion and Future Work

615 In the future, we will evaluate the proposed method on  
 616 other computer vision tasks such as single image super-  
 617 resolution, photo-sketch synthesis, and cross-domain im-  
 618 age recognition. Our proposed method can be improved  
 619 if we use better training images, fine tune the parameters  
 620 via cross-validation. We believe that our framework can  
 621 be useful not just for real image denoising, but for image  
 622 super-resolution, image cross-style synthesis, and recogni-  
 623 tion tasks. This will be our line of future work.

## References

- [1] A. Buades, B. Coll, and J. M. Morel. A non-local algorithm for image denoising. *CVPR*, pages 60–65, 2005. [1](#), [2](#), [3](#)
- [2] S. Roth and M. J. Black. Fields of Experts. *International Journal of Computer Vision*, 82(2):205–229, 2009. [1](#)
- [3] M. Elad and M. Aharon. Image denoising via sparse and redundant representations over learned dictionaries. *Image Processing, IEEE Transactions on*, 15(12):3736–3745, 2006. [1](#), [2](#), [3](#), [4](#)
- [4] K. Dabov, A. Foi, V. Katkovnik, and K. Egiazarian. Image denoising by sparse 3-D transform-domain collabora-  
tive filtering. *Image Processing, IEEE Transactions on*, 16(8):2080–2095, 2007. [1](#), [2](#), [3](#), [6](#)

<sup>1</sup>To compare with CCNoise, we first transform the denoised images into double format.



Figure 4. Denoised images of the image "Nikon D600 ISO 3200 C1" by different methods. The images are better to be zoomed in on screen.

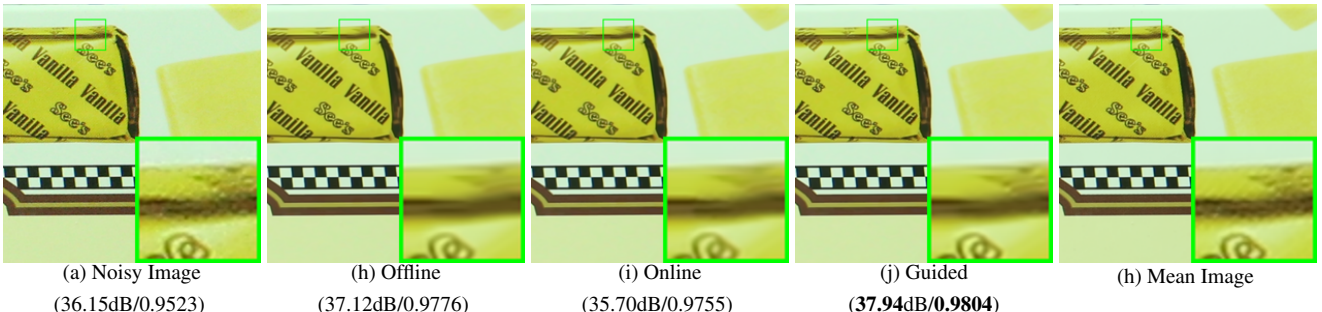


Figure 5. Denoised images of the image "Canon EOS 5D Mark3 ISO 3200 C1" by different methods. The images are better to be zoomed in on screen.

- [5] J. Mairal, F. Bach, J. Ponce, G. Sapiro, and A. Zisserman. Non-local sparse models for image restoration. *ICCV*, pages 2272–2279, 2009. [1](#), [2](#), [3](#)
- [6] D. Zoran and Y. Weiss. From learning models of natural image patches to whole image restoration. *ICCV*, pages 479–486, 2011. [1](#), [2](#)
- [7] Harold C Burger, Christian J Schuler, and Stefan Harmeling. Image denoising: Can plain neural networks compete with bm3d? *Computer Vision and Pattern Recognition (CVPR), 2012 IEEE Conference on*, pages 2392–2399, 2012. [1](#), [2](#), [6](#)
- [8] S. Gu, L. Zhang, W. Zuo, and X. Feng. Weighted nuclear norm minimization with application to image denoising. *CVPR*, pages 2862–2869, 2014. [1](#), [2](#), [3](#), [6](#)
- [9] U. Schmidt and S. Roth. Shrinkage fields for effective image restoration. *Computer Vision and Pattern Recognition (CVPR), 2014 IEEE Conference on*, pages 2774–2781, June 2014. [1](#), [2](#), [6](#)
- [10] J. Xu, L. Zhang, W. Zuo, D. Zhang, and X. Feng. Patch group based nonlocal self-similarity prior learning for image denoising. *2015 IEEE International Conference on Computer Vision (ICCV)*, pages 244–252, 2015. [1](#), [2](#), [3](#)
- [11] Yunjin Chen, Wei Yu, and Thomas Pock. On learning optimized reaction diffusion processes for effective image restoration. *Proceedings of the IEEE Conference on Computer Vision and Pattern Recognition*, pages 5261–5269, 2015. [1](#), [2](#), [6](#)
- [12] S. J. Kim, H. T. Lin, Z. Lu, S. Ssstrunk, S. Lin, and M. S. Brown. A new in-camera imaging model for color computer

vision and its application. *IEEE Transactions on Pattern Analysis and Machine Intelligence*, 34(12):2289–2302, Dec 2012. [1](#)

- [13] Seonghyeon Nam, Youngbae Hwang, Yasuyuki Matsushita, and Seon Joo Kim. A holistic approach to cross-channel image noise modeling and its application to image denoising. *Proc. Computer Vision and Pattern Recognition (CVPR)*, pages 1683–1691, 2016. [1](#), [2](#), [3](#), [5](#), [6](#), [8](#)
- [14] Glenn E Healey and Raghava Kondepudy. Radiometric ccd camera calibration and noise estimation. *IEEE Transactions on Pattern Analysis and Machine Intelligence*, 16(3):267–276, 1994. [1](#)
- [15] J. Portilla. Full blind denoising through noise covariance estimation using gaussian scale mixtures in the wavelet domain. *Image Processing, 2004. ICIP '04. 2004 International Conference on*, 2:1217–1220, 2004. [1](#), [3](#)
- [16] Tamer Rabie. Robust estimation approach for blind denoising. *Image Processing, IEEE Transactions on*, 14(11):1755–1765, 2005. [1](#), [3](#)
- [17] C. Liu, R. Szeliski, S. Bing Kang, C. L. Zitnick, and W. T. Freeman. Automatic estimation and removal of noise from a single image. *IEEE Transactions on Pattern Analysis and Machine Intelligence*, 30(2):299–314, 2008. [1](#), [3](#)
- [18] Zheng Gong, Zuowei Shen, and Kim-Chuan Toh. Image restoration with mixed or unknown noises. *Multiscale Modeling & Simulation*, 12(2):458–487, 2014. [1](#), [3](#)

756 Table 2. Average PSNR(dB) results of different methods on 60 cropped real noisy images captured in [13].  
757  
758  
759  
760810  
811  
812  
813  
814  
815  
816  
817  
818  
819  
820  
821  
822  
823  
824  
825  
826  
827  
828  
829  
830  
831  
832  
833  
834  
835  
836  
837  
838  
839  
840  
841  
842  
843  
844  
845  
846  
847  
848  
849  
850  
851  
852  
853  
854  
855  
856  
857  
858  
859  
860  
861  
862  
863

	Noisy	CBM3D	WNNM	MLP	CSF	TRD	NI	NC	Guided	Guided2
PSNR	34.51	34.58	34.52	36.19	37.40	37.75	36.53	37.57	38.72	38.90
SSIM	0.8718	0.8748	0.8743	0.9470	0.9598	0.9617	0.9241	0.9514	0.9694	0.9702

761 Table 3. Average PSNR(dB) results of different methods on 15 cropped real noisy images used in [13].  
762  
763

Camera Settings	Noisy	CBM3D	WNNM	MLP	CSF	TRD	NI	NC	CC	Guided2
Canon 5D Mark III ISO = 3200	37.00	37.08	37.09	33.92	35.68	36.20	37.68	38.76	38.37	40.50
	33.88	33.94	33.93	33.24	34.03	34.35	34.87	35.69	35.37	37.22
	33.83	33.88	33.90	32.37	32.63	33.10	34.77	35.54	34.91	37.13
Nikon D600 ISO = 3200	33.28	33.33	33.34	31.93	31.78	32.28	34.12	35.57	34.98	35.34
	33.77	33.85	33.79	34.15	35.16	35.34	35.36	36.70	35.95	36.69
	34.93	35.02	34.95	37.89	39.98	40.51	38.68	39.28	41.15	39.17
Nikon D800 ISO = 1600	35.47	35.54	35.57	33.77	34.84	35.09	37.34	38.01	37.99	38.82
	35.71	35.79	35.77	35.89	38.42	38.65	38.57	39.05	40.36	40.98
	34.81	34.92	34.95	34.25	35.79	35.85	37.87	38.20	38.30	38.90
Nikon D800 ISO = 3200	33.26	33.34	33.31	37.42	38.36	38.56	36.95	38.07	39.01	38.69
	32.89	32.95	32.96	34.88	35.53	35.76	35.09	35.72	36.75	36.82
	32.91	32.98	32.96	38.54	40.05	40.59	36.91	36.76	39.06	38.80
Nikon D800 ISO = 6400	29.63	29.66	29.71	33.59	34.08	34.25	31.28	33.49	34.61	33.31
	29.97	30.01	29.98	31.55	32.13	32.38	31.38	32.79	33.21	33.18
	29.87	29.90	29.95	31.42	31.52	31.76	31.40	32.86	33.22	33.35
Average PSNR	33.41	33.48	33.48	34.32	35.33	35.65	35.49	36.43	36.88	37.26
Average SSIM	0.8483	0.8511	0.8512	0.9113	0.9250	0.9280	0.9126	0.9364	0.9481	0.9505

- [784] M. Lebrun, M. Colom, and J.-M. Morel. Multiscale image  
785 blind denoising. *Image Processing, IEEE Transactions on*,  
786 24(10):3149–3161, 2015. 1, 2, 3, 5
- [787] Fengyuan Zhu, Guangyong Chen, and Pheng-Ann Heng.  
From noise modeling to blind image denoising. *The IEEE  
788 Conference on Computer Vision and Pattern Recognition  
789 (CVPR)*, June 2016. 1, 3
- [790] C. M. Bishop. *Pattern recognition and machine learning*.  
791 New York: Springer, 2006. 1
- [792] Z. Wang, A. C. Bovik, H. R. Sheikh, and E. P. Simoncelli.  
793 Image quality assessment: from error visibility to struc-  
794 tural similarity. *IEEE Transactions on Image Processing*,  
795 13(4):600–612, 2004. 1, 6
- [796] K. Dabov, A. Foi, V. Katkovnik, and K. Egiazarian. Color  
797 image denoising via sparse 3d collaborative filtering with  
798 grouping constraint in luminance-chrominance space. *IEEE  
799 International Conference on Image Processing*, 1, 2007. 2
- [800] Neatlab ABSoft. Neat image. [https://ni.  
801 neatvideo.com/home](https://ni.neatvideo.com/home). 2, 5, 6
- [802] G. Yu, G. Sapiro, and S. Mallat. Solving inverse problems  
803 with piecewise linear estimators: From Gaussian mixture  
804 models to structured sparsity. *IEEE Transactions on Image  
805 Processing*, 21(5):2481–2499, 2012. 2, 3
- [806] Daniel Glasner, Shai Bagon, and Michal Irani. Super-  
807 resolution from a single image. *ICCV*, 2009.
- [808] Maria Zontak, Inbar Mosseli, and Michal Irani. Separating  
809 signal from noise using patch recurrence across scales. *Pro-  
ceedings of the IEEE Conference on Computer Vision and  
Pattern Recognition*, pages 1195–1202, 2013.
- [810] Tomer Michaeli and Michal Irani. Blind deblurring using in-  
ternal patch recurrence. *European Conference on Computer  
Vision*, pages 783–798, 2014.
- [811] Y. Bahat and M. Irani. Blind dehazing using internal patch  
recurrence. *IEEE International Conference on Computa-  
tional Photography (ICCP)*, pages 1–9, May 2016.
- [812] J. Portilla, V. Strela, M.J. Wainwright, and E.P. Simoncelli.  
Image denoising using scale mixtures of Gaussians in the  
wavelet domain. *Image Processing, IEEE Transactions on*,  
12(11):1338–1351, 2003. 3
- [813] Peter J Huber. *Robust statistics*. Springer, 2011. 3
- [814] M. Lebrun, A. Buades, and J. M. Morel. A nonlocal bayesian  
image denoising algorithm. *SIAM Journal on Imaging Sciences*,  
6(3):1665–1688, 2013. 3
- [815] W. Dong, L. Zhang, G. Shi, and X. Li. Nonlocally central-  
ized sparse representation for image restoration. *Image Pro-  
cessing, IEEE Transactions on*, 22(4):1620–1630, 2013. 2,  
3
- [816] Chenglong Bao, Jian-Feng Cai, and Hui Ji. Fast sparsity-  
based orthogonal dictionary learning for image restoration.  
*Proceedings of the IEEE International Conference on Com-  
puter Vision*, pages 3384–3391, 2013. 4

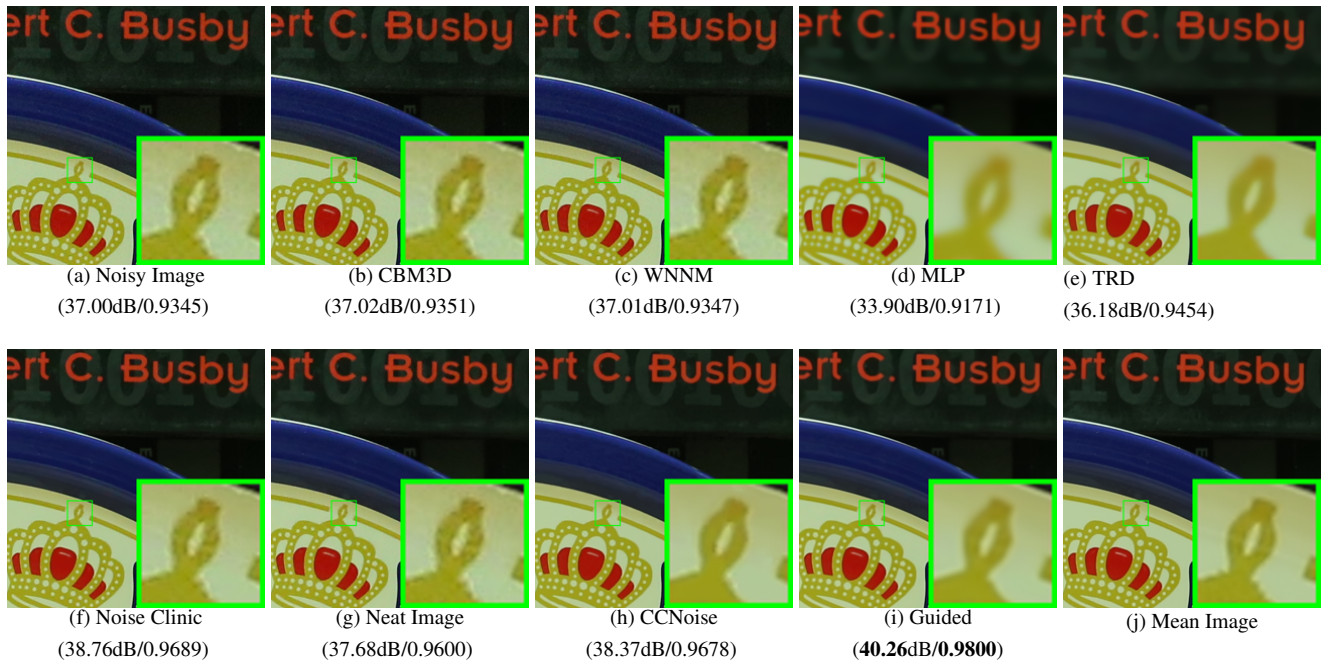


Figure 6. Denoised images of the image "Canon 5D Mark 3 ISO 3200 1" by different methods. The images are better to be zoomed in on screen.

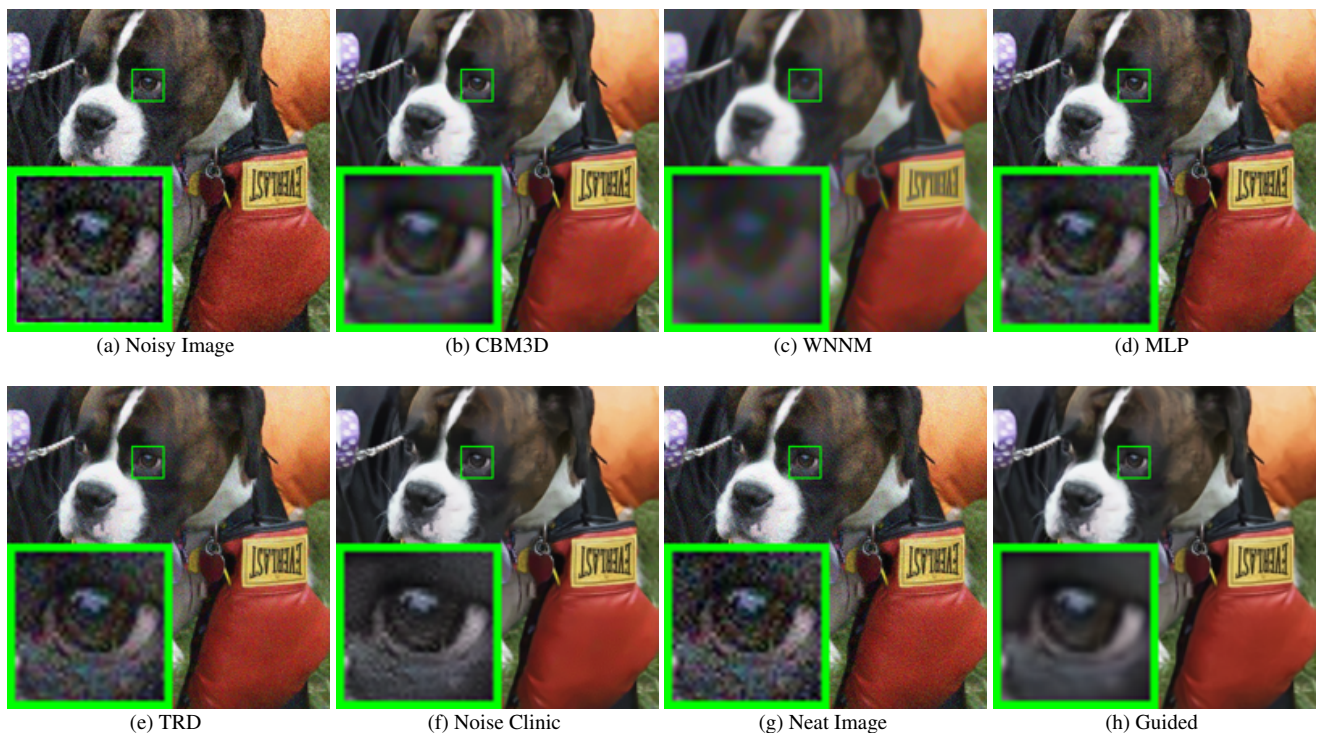


Figure 7. Denoised images of the image "5dmak3iso32003" by different methods. The images are better to be zoomed in on screen.

- [35] A. P. Dempster, N. M. Laird, and D. B. Rubin. Maximum likelihood from incomplete data via the EM algorithm. *Journal of the Royal Statistical Society. Series B (methodological)*, pages 1–38, 1977. 3, 4
- [36] David L Donoho and Michael Elad. Optimally sparse representation in general (nonorthogonal) dictionaries via 1 minimization. *Proceedings of the National Academy of Sciences*, 100(5):2197–2202, 2003. 3

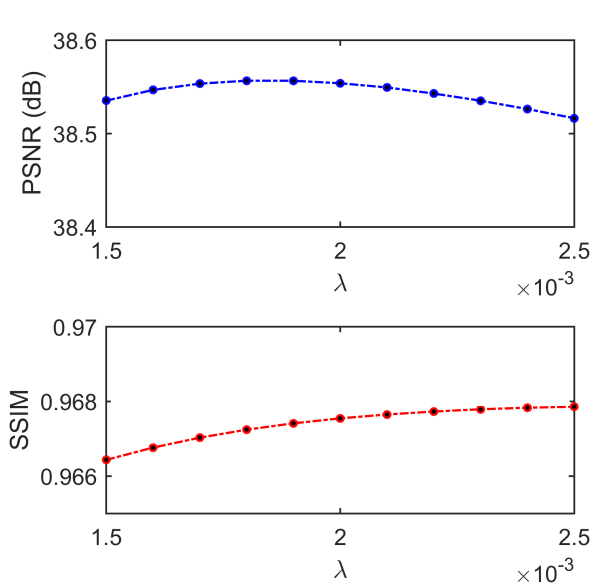


Figure 8. The PSNR/SSIM results as a function of the parameter  $\lambda$ .

- [37] Franklin C. Crow. Summed-area tables for texture mapping. *SIGGRAPH Comput. Graph.*, 18(3):207–212, January 1984. 5
- [38] Paul Viola and Michael J Jones. Robust real-time face detection. *International journal of computer vision*, 57(2):137–154, 2004. 5
- [39] S. Osher, M. Burger, D. Goldfarb, J. Xu, and W. Yin. An iterative regularization method for total variation-based image restoration. *Multiscale Modeling & Simulation*, 4(2):460–489, 2005. 5